PPPL-2254

MULTICHORD TIME-RESOLVED ELECTRON TEMPERATURE MEASUREMENTS BY THE X-RAY ABSORBER-FOIL METHOD ON TFTR

J. Kiraly,* M. Bitter, P. Efthimion, S. von Goeler,

B. Grek, K.W. Hill, D. Johnson, K. McGuire, N. Sauthoff,

S. Sesnic, F. Stauffer, G. Tait, and G. Taylor

Princeton University
Plasma Physics Laboratory
Princeton, NJ 08544 USA

PPPL--2254

DE85 017690

ABSTRACT

Absorber foils have been installed in the TFTR X-Ray Imaging System to permit measurement of the electron temperature along 10-30 chords spaced at 5-12.5 cm with a time resolution of less than 100 μs. The technique uses the ratio of X-ray fluxes transmitted through two different foils. The ratio depends mainly on electron temperature. Simulations show that strong impurity line radiation can distort this ratio. To correct for these effects, special beryllium-scandium filters are employed to select the line-free region between 2 and 4.5 keV. Other filter pairs allow corrections for Fe L and Ni L line radiation as well as Ti K and Ni K emission. Good accuracy is also obtained with simple beryllium filters, provided that impurity corrections are incorporated in the analysis, taking line intensities from the X-ray pulse-height analysis diagnostic. A description of modeling calculations and a comparison of temperature values from this diagnostic with data from the X-ray pulse height analysis, the electron cyclotron emission, and the Thomson scattering diagnostics are presented. Several applications of the absorber foil electron temperature diagnostic on TFTR are discussed. In particular, it was found in compression discharges that unusually large internal sawtooth disruptions occurred during or shortly after compression. The large sawteeth cause a redistribution of the plasma energy and may be partly responsible for deviations from adiabatic scaling.

*IAEA Fellow. Permanent address: Institute of Isotopes of the Hungarian Academy of Sciences, Budapest, Hungary.

INTRODUCTION

X-ray imaging arrays are an important diagnostic for magnetohydrodynamic (MHD) instabilities on most tokamaks. A selectable multifoil absorber system has provided the X-ray Imaging System (XIS)[1] of the Tokamak Fusion Test Reactor (TFTR) with the additional capability to measure electron temperature profiles by means of the two-foil technique.[2-6]

The X-ray Imaging System is essentially a one-dimensional slot-hole X-ray camera, illustrated schematically in Fig. 1. The plasma X-ray emission is viewed through a slot by an array of 64 silicon surface barrier diodes lying on a circular arc. The slot aperture is at the center of curvature of the arc. An individual detector views the plasma along a chord of tangent radius r. The current generated in the sensitive volume of a detector is proportional to the absorbed X-ray power. The spectral composition of the chordally integrated X-ray emission monitored by a given detector in the array depends on plasma parameters along the line of sight, such as the electron temperature $T_e(r)$, the electron density $n_e(r)$, and the concentration of impurities.[7,8] The spectral sensitivity of a detector is determined by the absorber foil, the detector dead layer, the detector material, and the depth of the depletion region. The basis of the absorber foil method is that the ratio of detector signals for two detectors with different absorbers depends mainly on the peak electron temperature along the chord. With suitably chosen absorber pairs, a comparison of the measured intensity ratios with numerical simulations, which account for profile effects and impurity line radiation, provides a measurement of the electron temperature T_e with very good time and spatial resolution.

The TFTR XIS hardware is described in Sec. I. Section II discusses briefly the simulation technique for the evaluation of the electron

temperature T_e. In Sec. III, a comparison with T_e measurements from other diagnostics and the first results with this diagnostic on compression and MHD fluctuations are presented.

I. THE TFTR X-RAY IMAGING SYSTEM

The silicon surface-barrier detectors of the horizontal XIS are arranged in two parallel rows; each row consists of 32 detectors. The detectors have a 7 × 30 mm^2 sensitive area and a 300 μm depletion layer thickness. In front of each row, there is a remotely controllable foil-ladder system permitting four choices of foils for every detector. The absorber foils are arranged on the foil ladder in such a fashion that the XIS system can be operated in two distinct modes. In the conventional imaging mode, beryllium foils are positioned in front of the detectors. The foil thickness varies for each row, and the operator can choose between the foil pair combinations 25 μm Be/125 μm Be or 125 μm Be/1250 μm Be. In the temperature mode, the following foils are put in an alternating sequence before the detectors: 25 μm Be + 5 μm Sc, 250 μm Be + 10 μm Sc, 125 μm Be + 5 μm Sc, 125 μm Be + 2.9 μm Ti, and 125 μm Be. The scandium and the titanium are coatings that are evaporated on the beryllium. The function of the scandium and titanium is to emphasize line-free regions of the X-ray spectrum with the help of absorption edges. This function will be explained in detail in the next section. The current generated in each detector of the array is amplified by a low-noise wide-band amplifier. The gain settings are separately programmable for all channels. Between shots, the leakage current of each detector is compensated by a feedback circuit which automatically zeros the preamplifier output. This servo loop is disabled just before a TFTR shot, and the leakage-current compensation remains constant for the duration of the discharge. The

amplified detector signals are sampled by transient digitizers with a selectable sampling rate up to 40 kHz, at present, and are stored in 2 k of local memory per channel. After the shot, the data are archived to a disk file. Presently, the TFTR XIS has 64 detectors and 40 electronic channels implemented. Additional electronic channels will be installed in the near future, as well as 60 fast digitizers with a 500 kHz maximum sampling rate. Figure 1 shows a schematic illustration of the X-ray Imaging System on TFTR. Figure 2 shows the diagram of one channel of the XIS signal processing and data acquisition electronics. Figure 3 is a photograph of the XIS installed on TFTR.

II. THEORY

The plasma X-ray emission is a superposition of bremsstrahlung, recombination radiation, and impurity line radiation. The local X-ray emissivity and the spectral composition of the radiation are determined by such quantities as the electron temperature, the electron density, the impurity concentrations, and the charge-state distributions of the impurities; the last one, in turn, depends on electron density, electron temperature, and impurity transport.[7] The slope of the radiated power as a function of photon energy on a semilogarithmic plot is inversely proportional to the electron temperature. Thus, one can determine the electron temperature of the plasma by comparing the X-ray intensity transmitted through two filters having different low-energy cutoffs with simulations. The computation of the temperature has to take into account the fact that the measured radiation is integrated along the line of sight of a detector. In addition, corrections have to be made for the effect of impurity line radiation.

The choice of absorber foils for the T_e measurement was influenced by several criteria: (1) The transmitted intensity ratio should vary sufficiently with T_e to give adequate sensitivity to T_e changes; (2) the transmission bands should exclude strong impurity L and K line radiation; and (3) enough radiation power should be transmitted to produce a sufficiently high detector signal-to-noise ratio. In order to optimize the XIS filters according to these criteria and in order to generate signal ratios for different filter combinations as a function of peak temperature and impurity concentration along a chord, a computer model was used.

The continuum radiation was approximated by a bremsstrahlung formula,

$$\frac{\Delta W}{\Delta E} \sim n_e^2(r)\ [T_e(r)]^{-1/2} \exp[-E/T_e(r)], \qquad (1)$$

where ΔW is the power radiated in the photon energy interval ΔE. In order to calculate the detector signal, we numerically integrate Eq. (1) over photon energy and along the detector line of sight ℓ, taking into account the effects of absorbers and detector dead layers as well as the detector spectral sensitivity,

$$I_{det} \sim \int_{\ell} \int_{E} \frac{n_e^2(\ell)}{T_e^{1/2}(\ell)} \exp\,[-E/T_e(\ell)]\ \exp\,[-\Sigma_i\ \mu_i(E)\ x_i]$$

$$\times \left\{1 - \exp[-\mu_{Si}\ (E)\ x_{Si}]\right\} I(E,\ell)\ dE\ d\ell, \qquad (2)$$

where $\mu_i(E)$ is the absorption coefficient[9] of the i-th absorber at photon energy E, x_i is the absorber thickness, and μ_{Si} is the absorption coefficient of silicon. $I(E,\ell)$ is a function which represents the relative intensity of impurity lines to the continuum at a position along the line of integration. Electron density and temperature profiles are assumed to be parabolas raised to the powers α and β, respectively, i.e., $n_e(r) = n_o (1 - r^2/a^2)^\alpha$ and $T_e(r) = T_o (1 - r^2/a^2)^\beta$. Although values of α and β inferred from other diagnostics may range from 0.5 to 3, the values $\alpha = 1$ and $\beta = 2$ were used in most of the measurements because the ratio of detector signals depends mainly on the peak temperature value along the chord and is relatively insensitive to the profile shape of temperature and density and to the tangent radius. The measurement, however, can be appreciably affected by intense impurity (Ti, Cr, Fe, Ni) K line radiation. At line-averaged electron densities $\bar{n}_e$ below 2×10^{19} m^{-3}, the impurity peaks generally are so large that they give a significant contribution to the X-ray signal for foils with a low energy cutoff above 3 keV. Two techniques are used to account for this effect. One is to include in the simulation measured line-to-continuum ratios from the X-ray pulse-height analysis (PHA) diagnostic.[7,10] The second technique is to include matched Ross filter pairs,[13] which have a well-known sensitivity to specific line radiation, on the foil ladder in order to obtain a direct measurement of that part of the radiation that originates from impurity lines.

The important impurity lines are shown in Fig. 4, which represents a typical X-ray PHA spectrum for a low density discharge in TFTR. Generally, there is a region, free from impurity lines, between $h\nu = 2$ keV and 4.5 keV. Below 2 keV, iron and nickel L lines distort the spectrum; above 4.5 keV, the titanium K_α line is very strong. Sulphur and chlorine lines appear between 2 keV and 3 keV but are expected to decrease in intensity with time as the

machine cleans up. The basic idea is to use the line-free region between 2 and 4.5 keV for temperature measurements. The Ti K radiation and the Ni L and Fe L radiation are independently measured and are used to correct the temperature measurements. In order to accomplish this goal, special scandium filters have been designed (125 μm Be + 5 μm Sc, 250 μm Be + 10 μm Sc, 25 μm Be + 5 μm Sc) which block the titanium radiation because of the scandium K absorption edge, and which are sufficiently thick to impede the low energy Ni L and Fe L radiation. The 25 μm Be and 125 μm Be filters are most sensitive in the energy region between 1.5 and 2 keV and will be used to determine the Ni-L and Fe-L radiation. In addition, these filters can be used for electron temperature determination at low temperatures (i.e., at the outer radii) where the Ni L and Fe L radiation tends to be unimportant. The balanced Ross filter pair[13] (125 μm Be + 5 μm Sc and 125 μm Be + 2.9 μm Ti) is used to measure the intensity of Ti K radiation. (The Ti K line is located between the absorption edges of Ti and Sc.) Since the impurity concentrations decrease sharply with n_e, the K line can be neglected at higher electron density, and the 125 μm Be/1250 μm Be pair can be used for the central electron temperature measurement without corrections, due to the line radiation in the high density region.

Figures 5, 6, and 7 show the calculated detector sensitivity (absorption in the sensitive layer of detector) as a function of photon energy for detectors filtered by various foils installed in the TFTR XIS system. Figure 5 represents the normal Be filters used in the XIS. Most of the measurements were performed with this set of foils. Figure 6 shows combination sets of beryllium and scandium. The purpose of these filters is to deemphasize the spectral region above 4.5 keV, where the titanium, chromium, iron, and nickel K lines are located. Scandium has a K edge at

4.49 keV, and the X-ray transmission is significantly reduced above that energy. Figure 7 displays the transmission characteristics of the balanced filter pair for the determination of the Ti concentration. Figure 8 shows the calculated detector response (energy absorption in the sensitive layer of the detector) as a function of photon energy for Be filters of different thicknesses at 1 keV, 2 keV, and 3 keV electron temperature. These curves illustrate which part of the X-ray spectrum gives the largest contribution to the detector current measured with a particular foil. Figure 9 shows the ratio of detector signals as a function of electron temperature, using 125 μm and 1250 μm Be foils, calculated by the model described above. From this and similar graphs, the electron temperature is deduced. The four curves illustrate the effect of various metal impurity concentrations on the T_e measurement. The curve with the open triangles represents a case of strong line contamination in TFTR. Under these unfavorable circumstances, the error in the temperature measurement without impurity corrections can be as large as a factor of almost two. The parameter of the curves in Fig. 9 is the ratio of line intensity to continuum intensity. This ratio is proportional to the impurity concentration in lowest order. So long as the impurity concentration does not change, the double foil temperature represents a fairly accurate measurement, particularly for relative changes, because the slope of the curve does not show appreciable variation with impurity content.

III. EXPERIMENTAL RESULTS

Preliminary electron temperature measurements have been made for a number of chords using the 125 μm and 1250 μm Be filter pair. The absorber foil T_e diagnostic played an important role on TFTR when the time evolution of the central electron temperature was studied during plasma compression

experiments,[11] and we consequently will use data from these discharges to demonstrate the usefulness of the diagnostic. Figure 10 shows the time evolution of the central electron temperature T_e for two discharges when a plasma with major radius R = 3.0 m, minor radius a = 0.55 m, plasma current I_p = 400 kA, and electron density $\bar{n}_e = 2 \times 10^{19}$ m^{-3} was adiabatically compressed during a time of approximately 20 ms to a discharge with R = 2.1 m, a = 0.53 m, I_p = 600 kA, and $\bar{n}_e = 3.3 \times 10^{19}$ m^{-3}. The compression was initiated at time t = 2.5 sec. An initial temperature increase of ~ 700 eV is observed at time t = 2.52 sec. The peak temperature after the compression is close to the value predicted by adiabatic scaling.[11] A rapid temperature decrease of 300-400 eV follows, which coincides with a large "sawtooth" relaxation in the soft X-ray emission. The two graphs of Fig. 10 depict situations with different phasing of the compression with respect to the sawtooth activity. In the top graph, the compression takes place after the sawtooth crash, whereas in the bottom graph it occurs before the crash. A three-dimensional display of these events is given in Fig. 11b, which shows the time evolution of the soft X-ray profile during compression measured by detectors filtered with 125 μm Be. The fact that the central stored plasma energy was rearranged at a sawtooth oscillation was less visible on other fast electron-temperature diagnostics, such as the fast-scanning electron-cyclotron emission (ECE) radiometer, because the plasma center was moving rapidly in major radius, complicating interpretation of the ECE data. For the X-ray measurement, the plasma center stays on the line of sight of the central detectors, and the temperature evaluation is independent of plasma position in first order. The ECE emission in Fig. 10 is averaged over 50 ms; the actual time resolution of the scanning radiometer on TFTR is 4 ms (this graph does not do justice to the true measuring capability of the ECE diagnostic).

Without correction for impurity K-line radiation, the T_e values from the absorber foil method agree well, in general, with the values measured by other diagnostics like the Thomson scattering measurement or the various ECE measurements (shown in Fig. 10). The somewhat higher values from the foil method after t ≈ 2.55 sec are due to increasing impurity line radiation which was negligible before this time.[12] The time evolution of the spatial temperature profile from five XIS chords is shown in Fig. 11a. The flattening of the T_e profile after the large sawtooth drop demonstrates the rapid expulsion of energy from the center to the outside of the plasma column. A similar situation, where unusually large sawtooth disruptions affect the transport, occurred in a TFTR discharge scenario that involved a weak compression from R = 3.05 m to 2.5 m, followed by a free expansion. The relevant XIS data are shown in Fig. 12.

The effect of impurity K_α lines on the absorber foil temperature data is demonstrated by the results in Fig. 13, which were taken during a steady-state, low-density discharge (I_p = 1 MA, $\bar{n}_e = 1.1 \times 10^{19}$ m^{-3}), where these effects were particularly severe. The double foil temperature measurement shown in Fig. 13b was performed with 125 μm and 1250 μm beryllium foils and was corrected for the K_α lines. The relative line-to-continuum intensity ratios were taken from the PHA spectrum of Fig. 13a for this same shot and were included in the simulation. The XIS results agree well with the PHA T_e measurement of 3.0 keV in the 2.5-3 sec interval and with the ECE measurement shown in Fig. 13c. For this case, with an intense impurity line contribution, the uncorrected XIS T_e values are too high by about a factor of two. Figure 13d shows the sawtooth modulation of the T_e profile measured by the XIS for the same shot in the time interval 2.5 - 2.65 sec.

Another situation, where rapid temperature changes occur and where the XIS temperature has been very useful, is during neutral beam injection. Figure 14, for example, shows the central electron temperature measured by the XIS for a shot with 1.5 MW neutral beam injection in the time interval 2.3 - 2.8 sec into a discharge with I_p=1 MA, $\bar{n}_e$=2.0 × 10^{19} - 2.4 × 10^{19} m^{-3}. The modulation on the XIS trace is again due to sawtooth oscillations. The figure also shows the electron-temperature values measured by the PHA which agree well with the values measured by the XIS.

The most important role for the XIS temperature measurement will be in the study of MHD fluctuations and disruptions, where rapid temperature changes and radial in-out motions occur. Figure 15 shows a comparison of the central electron temperature evolution measured by different diagnostics for a disruptive shot. The main disruption occurs at approximately 700 ms. The resulting temperature decay entails several secondary disruptions, e.g., at ~ 1200 ms, ~ 1420 ms, etc. The temperature values given by the absorber-foil method using the scandium filters are again in very good agreement with other methods over a wide temperature range (1-5 keV). The slightly higher XIS data after 1000 ms are due again to the fact that no impurity correction has been applied for computing the XIS temperature.

IV. CONCLUSIONS

Simulation codes have been developed to permit electron temperature profile measurements by the two-absorber method with the existing TFTR X-ray Imaging System. The potential time resolution is 2 μs, and the spatial resolution is approximately 5 cm. The fast time resolution and multichord capability may permit studies of phenomena involving fast T_e profile evolution previously inaccessible to researchers. Preliminary results look promising.

The absorber foil diagnostic has been particularly useful during plasma compression discharges on TFTR, where it has been shown that internal sawtooth disruptions occurred after the compression and caused a strong relaxation of the temperature profile. The measured, central temperature increases in agreement with adiabatic scaling before the internal disruption, but it lies considerably below the theoretically predicted values after disruption. A careful analysis of the transport including sawtooth effects and a systematic investigation of different discharge conditions has not yet been performed, so it is not clear to what extent the sawteeth are responsible for the deviations from adiabatic scaling reported in Ref. 11.

From the diagnostic point of view, more detailed comparisons with other diagnostics over a wide range of temperatures and densities for different impurity levels and with a variety of profiles are needed to check the simulations and the impurity corrections. Recently installed additional electronic channels to utilize all 64 detectors and faster transient digitizers (up to 500 kHz) will permit a more complete realization of the multichord and fast time resolution capabilities of this diagnostic.

ACKNOWLEDGMENTS

The authors gratefully acknowledge the continuing support of Drs. H.P. Furth, P. Rutherford, D. Grove, D.M. Meade, K. Young, and L.C. Johnson. The work of E. Mooney, J. Gorman, J. Lehner, and D. Moore during design, fabrication, and assembly of the TFTR X-ray Imaging System, and the technical support of the TFTR operating crew are appreciated.

This work was supported by U.S. Dept. of Energy Contract No. DE-AC02-76-CHO-3073.

REFERENCES

[1]K.W. Hill, S. von Goeler, M. Bitter, W. Davis, L. Dudek, E. Fredd, L.C. Johnson, J. Kiraly, K. McGuire, J. Montague, E. Moshey, N. R. Sauthoff, and K.M. Young, Rev. Sci. Instrum. 56, 830 (1985).

[2]T.P. Donaldson, Plasma Phys. 20, 1279 (1978).

[3]F.C. Jahoda, E.M. Little, W.E. Quinn, G.A. Sawyer, and T.F. Stratton, Phys. Rev. 119, 843 (1960).

[4]R. Bardet, Measure de la temperature electronique d'un plasma, a partir du rayonnement X, par la technique des absorbents, Fontenay-aux-Roses report EUR-CEA-FC-1038 (1980), (unpublished).

[5]J. Kiraly, M. Bitter, S. von Goeler, K.W. Hill, L.C. Johnson, K. McGuire, S. Sesnic, N.R. Sauthoff, F. Tenney, and K.M. Young, Rev. Sci. Instrum. 56, 827 (1985).

[6]J. Kiraly, M. Bitter, S. von Goeler, K.W. Hill, K. McGuire, S. Sesnic, N.R. Sauthoff, and F. Tenney, Bull. Am. Phys. Soc. APS 29, 1304 (1984).

[7]S. von Goeler, in Diagnostics for Fusion Experiments, E. Sindoni and C. Wharton editors, (Pergamon Press, New York, 1979).

[8]S. von Goeler, W. Stodiek, H. Eubank, H. Fishman, S. Grebenschikov, and E. Hinnov, Nucl. Fusion 15, 301 (1975).

[9]F. Biggs and R. Lighthill, Sandia Laboratories Report SC-RR-710507 (1971) (unpublished).

[10]K.W. Hill, M. Bitter, M. Diesso, L. Dudek, S. von Goeler, S. Hayes, L.C. Johnson, J. Kiraly, E. Moshey, G. Renda, S. Sesnic, N.R. Sauthoff, F. Tenney, and K.M. Young, Rev. Sci. Instrum. 56, 840 (1985).

[11]G. Tait *et al.*, Proc. 10th Int. Conf. on Plasma Physics and Contr. Thermonucl. Fusion, London (IAEA, Vienna, 1985), Vol. 1, p. 141.

[12]P.H. Tenney, K.W. Hill, S. Sesnic, B. Grek, D.W. Johnson, J.F. Schivell, G.D. Tait, Bull. Am. Phys. Soc. APS 29, 1384 (1984).

[13]P.A. Ross, Phys. Rev. 28, 425 (1926); P. Kirkpatrick, Rev. Sci. Instrum. 10, 186 (1939) and Rev. Sci. Instrum. 15, 223 (1944).

FIGURES

Fig. 1 Schematic illustrations of the X-ray Imaging System (XIS) installed on TFTR. Detector lines of sight are depicted for large plasma and pre- and post-compression plasmas. The indicated neutron and gamma-ray shielding will be added in the future.

Fig. 2 Schematic diagram of one channel of the XIS signal processing and data acquisition electronics.

Fig. 3 Photo of the X-ray Imaging System installed on the TFTR tokamak. Preamplifiers and cables which connect the preamplifiers to amplifiers in the data acquisition room can be seen, as well as the vacuum equipment.

Fig. 4 X-ray spectrum from TFTR plasma measured by the X-ray pulse-height analysis system showing the exponentially decreasing continuum from which electron temperature is measured and K lines from metal impurities which can affect the two-foil temperature measurements.

Fig. 5 Calculated detector sensitivity (ratio of photons absorbed in the sensitive layer of the detector to incident photons) as a function of photon energy for detectors with different beryllium filters.

Fig. 6 Calculated detector sensitivity as a function of photon energy for detectors with different beryllium-scandium filters.

Fig. 7 Detector sensitivity as a function of photon energy for the filter pair (125 µm Be + 5 µm Sc and 125 µm Be + 2.9 µm Ti) to measure the Ti K_α line radiation.

Fig. 8 The spectral contribution of the plasma continuum radiation to the detector signal for different electron temperatures and for different beryllium filters.

Fig. 9 Ratios of detector signals computed according to Eq. (2) for detectors with 1250 µm and 125 µm Be filters, as a function of electron temperature for different impurity line radiation. The label of the curve indicates the type and the amount of line contamination of the spectrum. The numbers represent the ratio line height over continuum from the X-ray PHA spectrum.

Fig. 10 Time history of the central electron temperature measured by different diagnostics for strong compression discharges R = 3.05 to 2.17 m. The values from the absorber foil method using the 125 µm and the 1250 µm Be pair show that the peak temperature after the compression is close to the value predicted by adiabatic scaling, but is followed by a sharp drop of 300-400 eV which coincides with a large sawtooth relaxation in the soft X-ray emission.

Fig. 11a Time evolution of spatial T_e profile from five chords measured by XIS for the same shot as in Fig. 10. The flattening of the T_e profile after the large sawtooth drop demonstrates the rapid expulsion of energy from the center to the outside of the plasma column. Detector position 25 corresponds to a minor radius of 32 cm before compression and to 48 cm after compression.

Fig. 11b Time evolution of the line integrated soft X-ray profile measured by detectors filtered with 125 μm Be for a compression shot.

Fig. 12 Time history of the central electron temperature measured by different diagnostics for weak compression discharges R = 3.05 to 2.5 m followed by free expansion. The temperature evolution measured with the absorber foil method, using the 125 μm and the 1250 μm Be pair, again shows a sharp drop of 300-400 eV which coincides with a large sawtooth relaxation in the soft X-ray emission.

Fig. 13a — X-ray spectrum from a TFTR low density ($\bar{n}_e = 1.1 \times 10^{19}$ m^{-3}) discharge measured by the pulse-height-analysis system showing the strong Ti, Cr, Fe, and Ni impurity K-line radiation which affect the absorber-foil temperature measurement.

Fig. 13b–13c — Comparison of central T_e vs time measured by (b) XIS and (c) ECE radiometer for same discharge as in Fig. 13a. Correction for impurity lines with relative intensity as shown in Fig. 13a reduces the ratio by ~ 50% so that it agrees well with the ECE temperature, and with the PHA value of 3.0 keV measured in the 2.5 - 3 sec interval.

Fig. 13d — Electron temperature vs tangent radius and time for the same discharge as in Figs. 13a, 13b, and 13c.

Fig. 14 — The central electron temperature measured by XIS for a shot with 1.5 MW neutral beam injection in the time interval 2.3 - 2.8 sec. $I_p = 1$ MA, $\bar{n}_e = 2.0 \times 10^{19} - 2.4 \times 10^{19}$ m^{-3}. The figure also shows the electron temperature values measured by the PHA, which agree well with the values measured by the XIS.

Fig. 15 — Comparison of the central electron temperature evolution measured by different diagnostics for a disruptive shot. The T_e values given by the XIS agree very well in wide T_e range (1-5 keV) with the values from other methods.

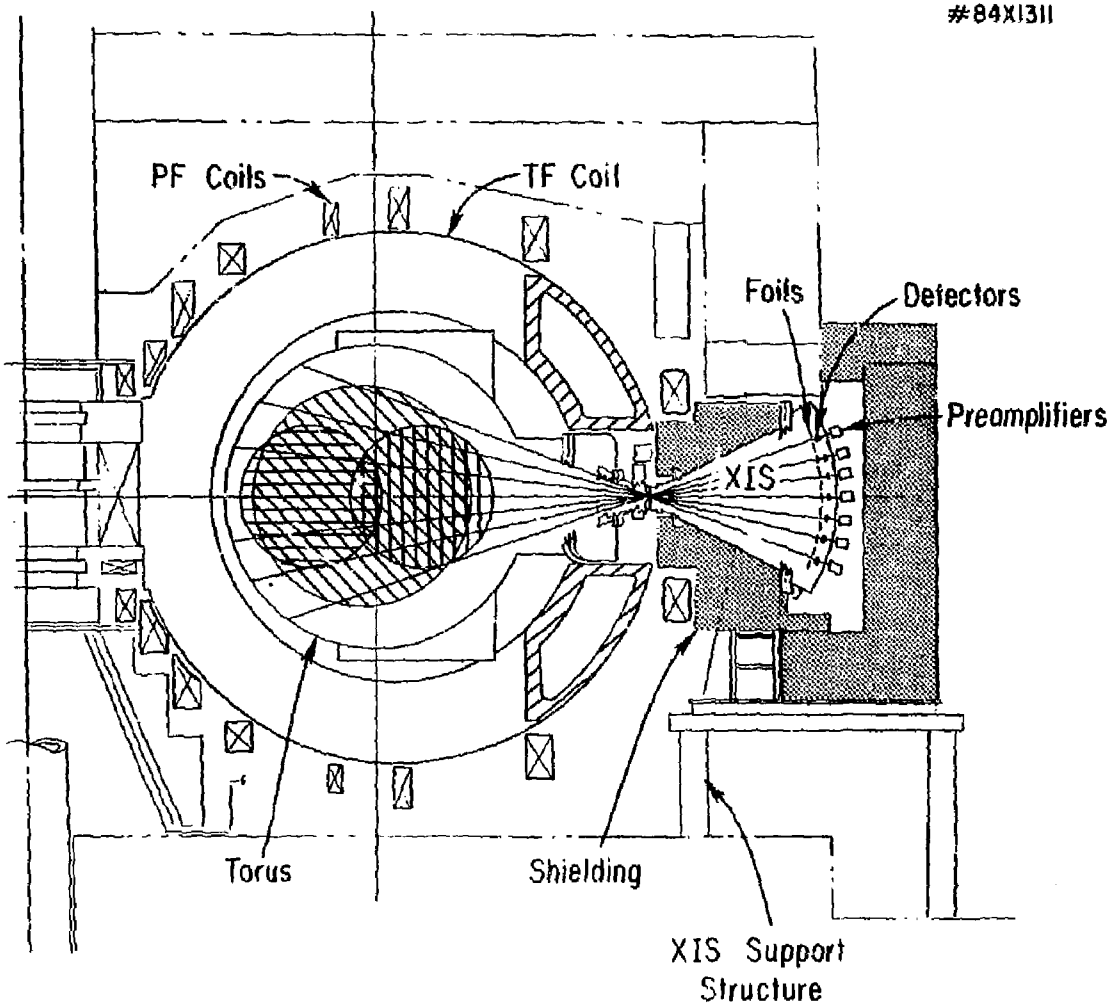
#84X1311
PF Coils
TF Coil
Foils
Detectors
Preamplifiers
XIS
Torus
Shielding
XIS Support
Structure

Fig. 1

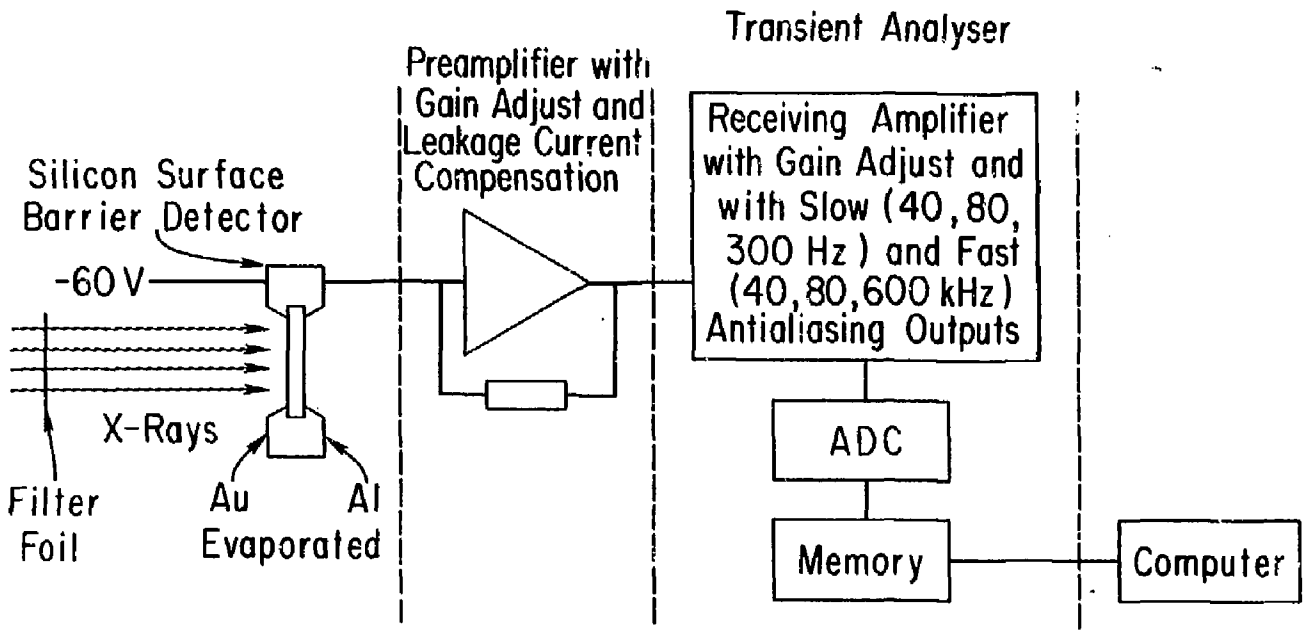
Transient Analyser
Preamplifier with Gain Adjust and Leakage Current Compensation
Silicon Surface Barrier Detector
-60 V
Receiving Amplifier with Gain Adjust and with Slow (40, 80, 300 Hz) and Fast (40, 80, 600 kHz) Antialiasing Outputs
X-Rays
ADC
Filter Foil
Au Evaporated
Al
Memory
Computer

Fig. 2

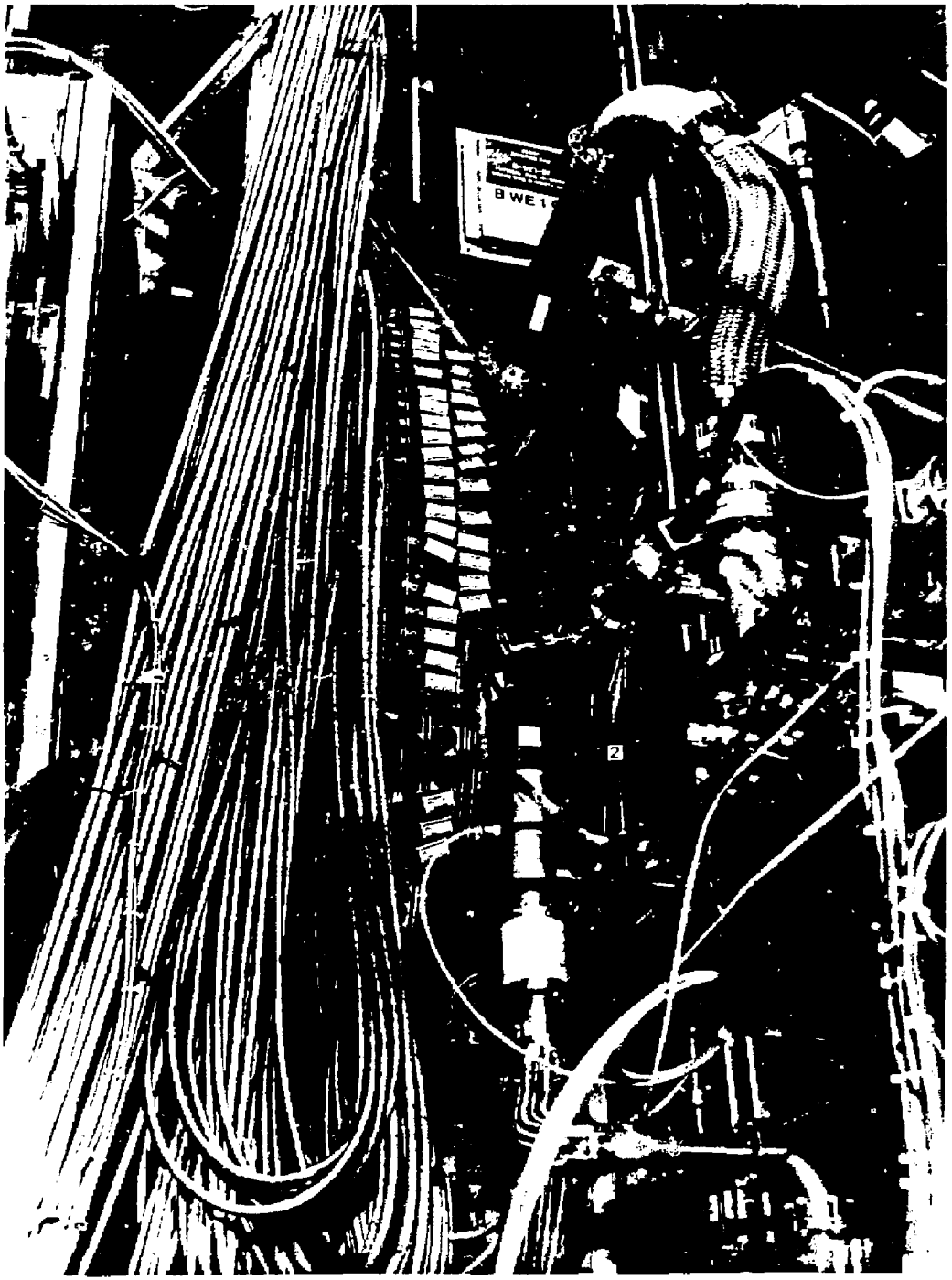

Fig. 3

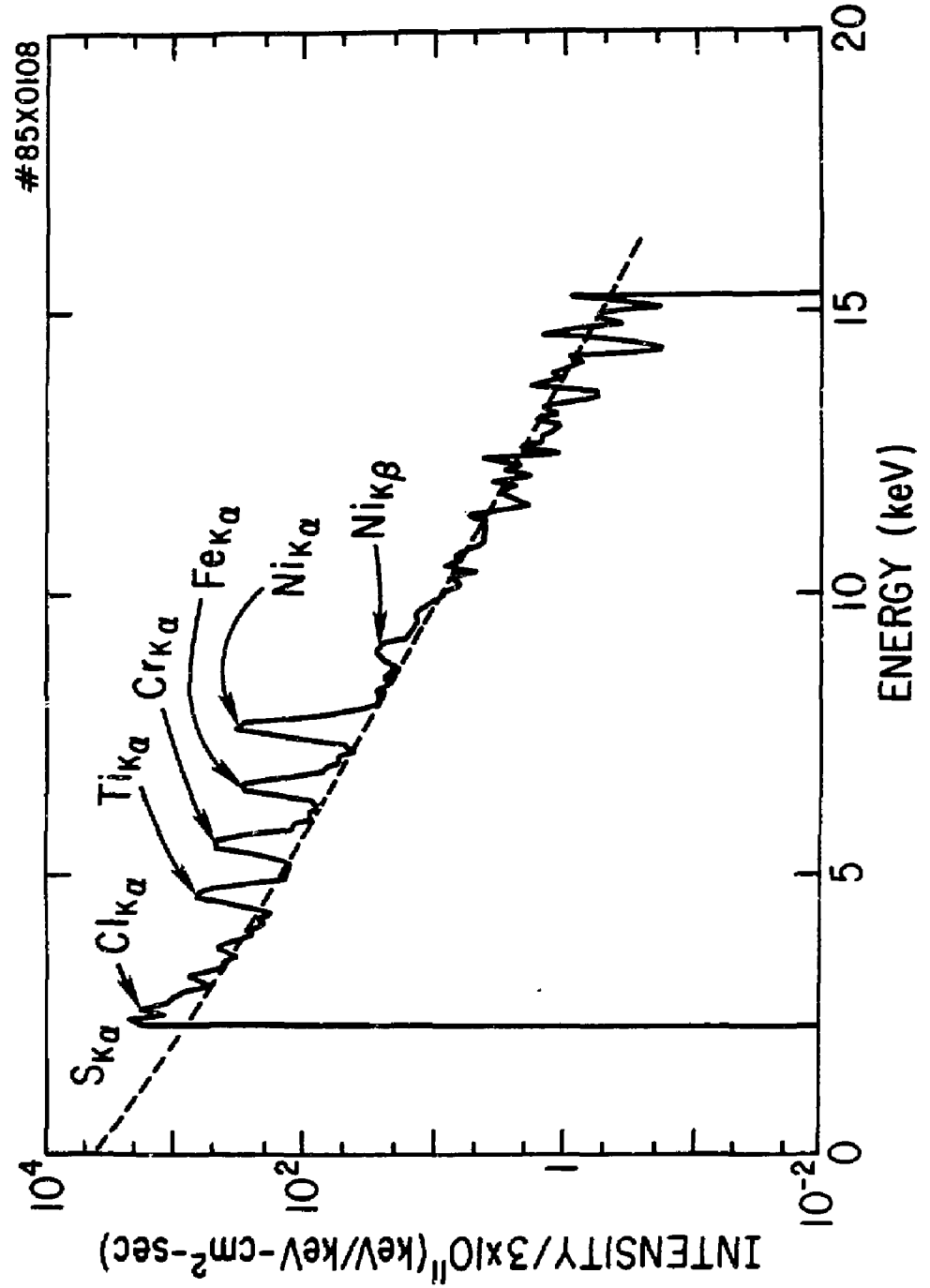
#85X0108
INTENSITY/3x10^11(keV/keV-cm^2-sec)
ENERGY (keV)
10^4
10^2
1
10^-2
0
5
10
15
20
S Kα
Cl Kα
Ti Kα
Cr Kα
Fe Kα
Ni Kα
Ni Kβ

Fig. 4

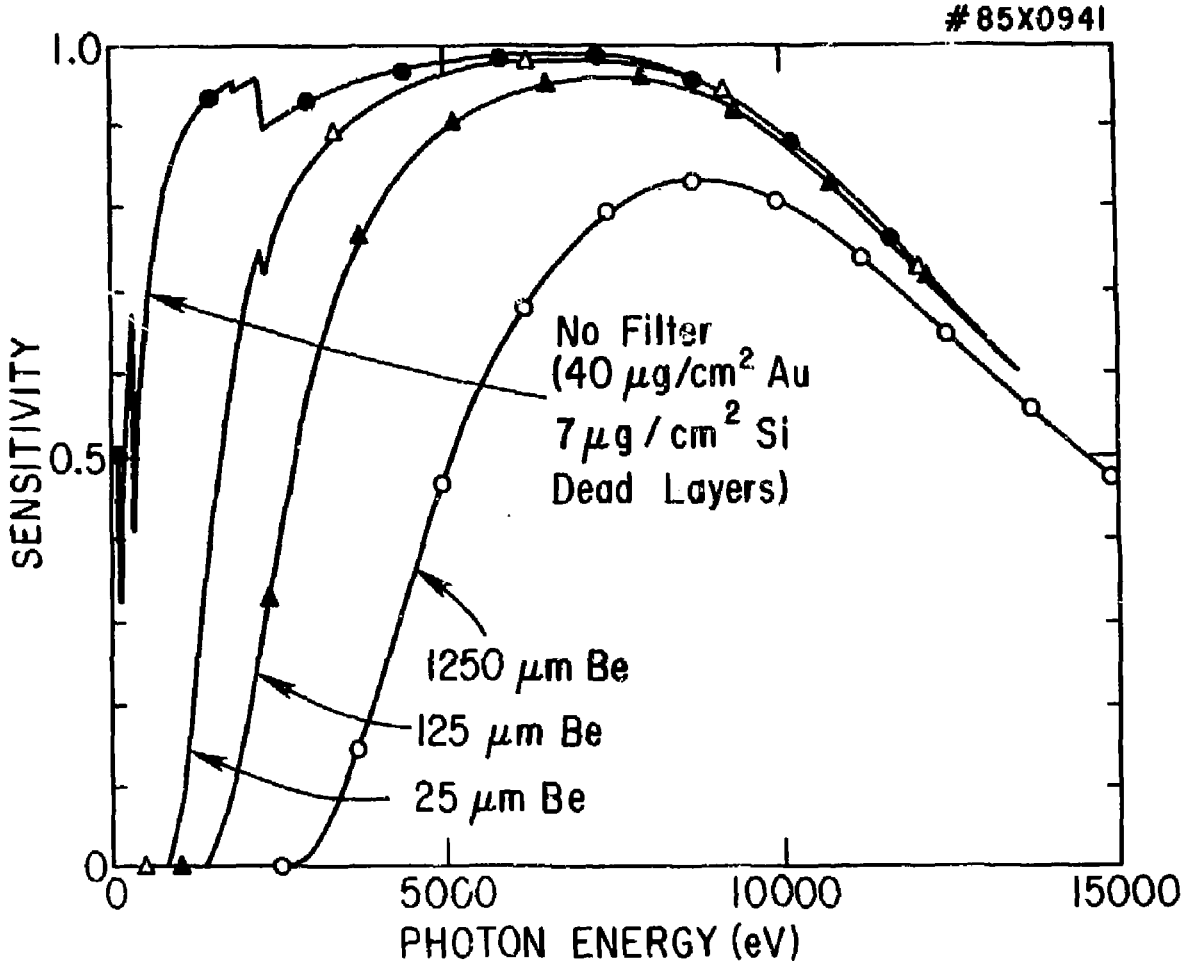
#85X0941
1.0
0.5
0
SENSITIVITY
No Filter
(40 μg/cm² Au
7 μg/cm² Si
Dead Layers)
1250 μm Be
125 μm Be
25 μm Be
0
5000
10000
15000
PHOTON ENERGY (eV)

Fig. 5

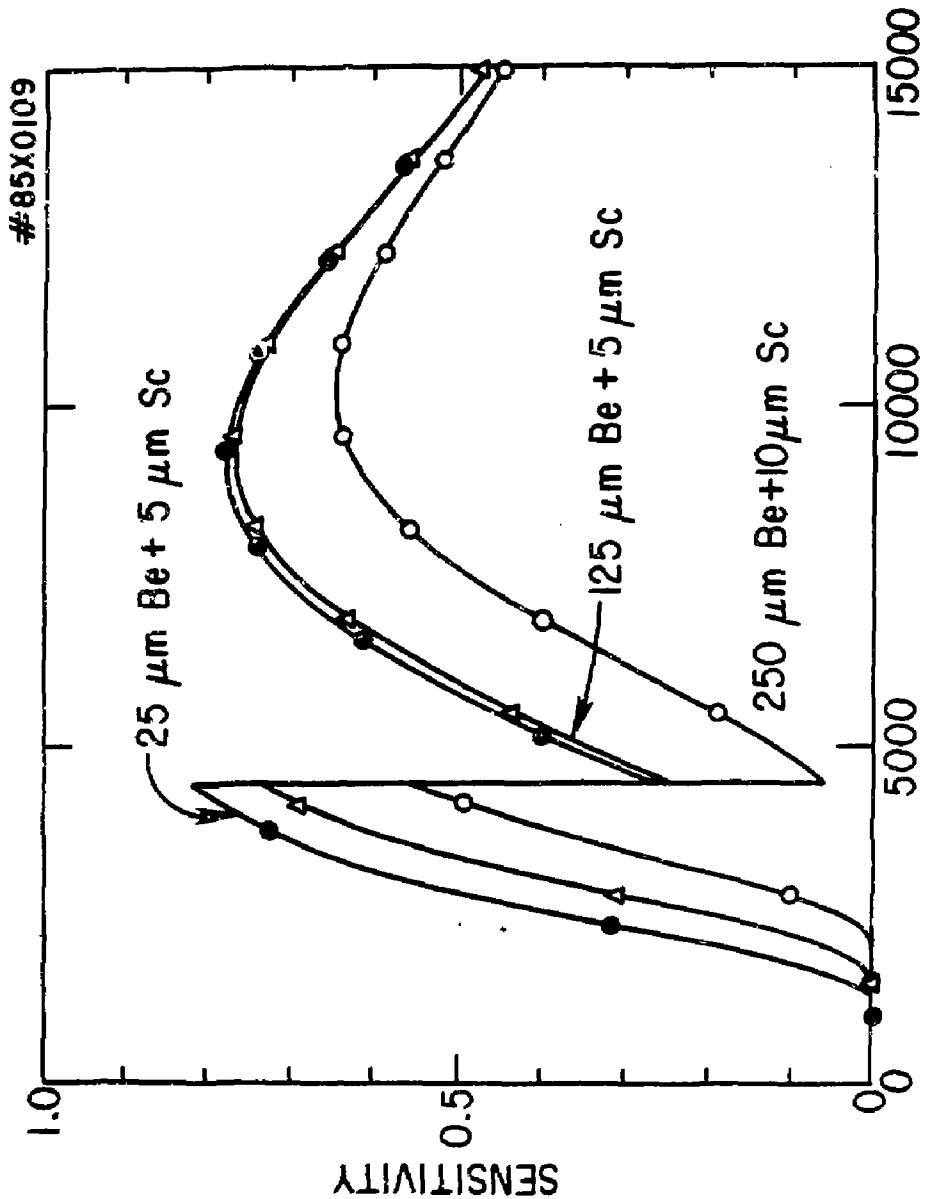
#85X0109
25 μm Be + 5 μm Sc
125 μm Be + 5 μm Sc
250 μm Be+10μm Sc
SENSITIVITY
1.0
0.5
0
0
5000
10000
15000
PHOTON ENERGY (eV)

Fig. 6

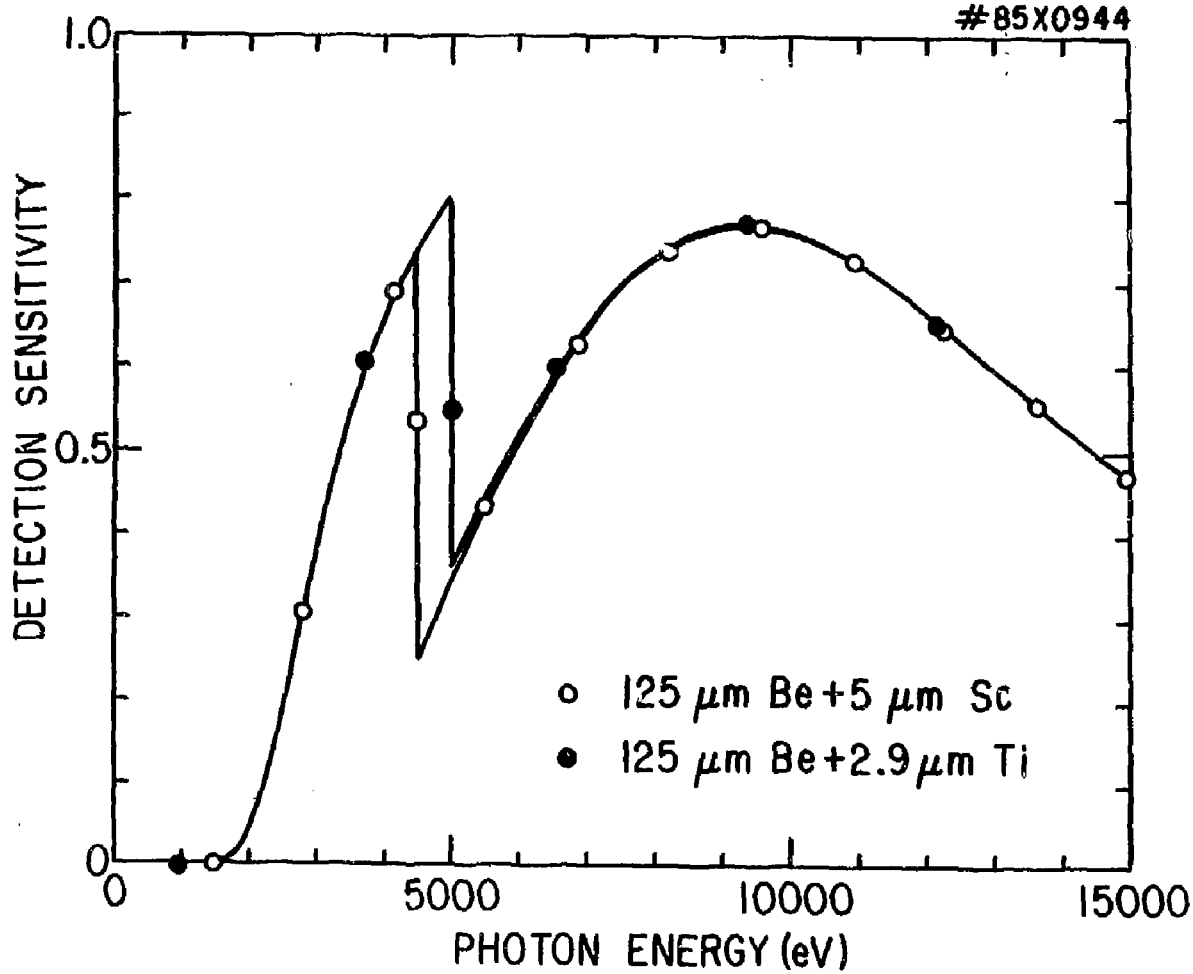
#85X0944
1.0
0.5
0
DETECTION SENSITIVITY
0
5000
10000
15000
PHOTON ENERGY (eV)
125 μm Be+5 μm Sc
125 μm Be+2.9 μm Ti

Fig. 7

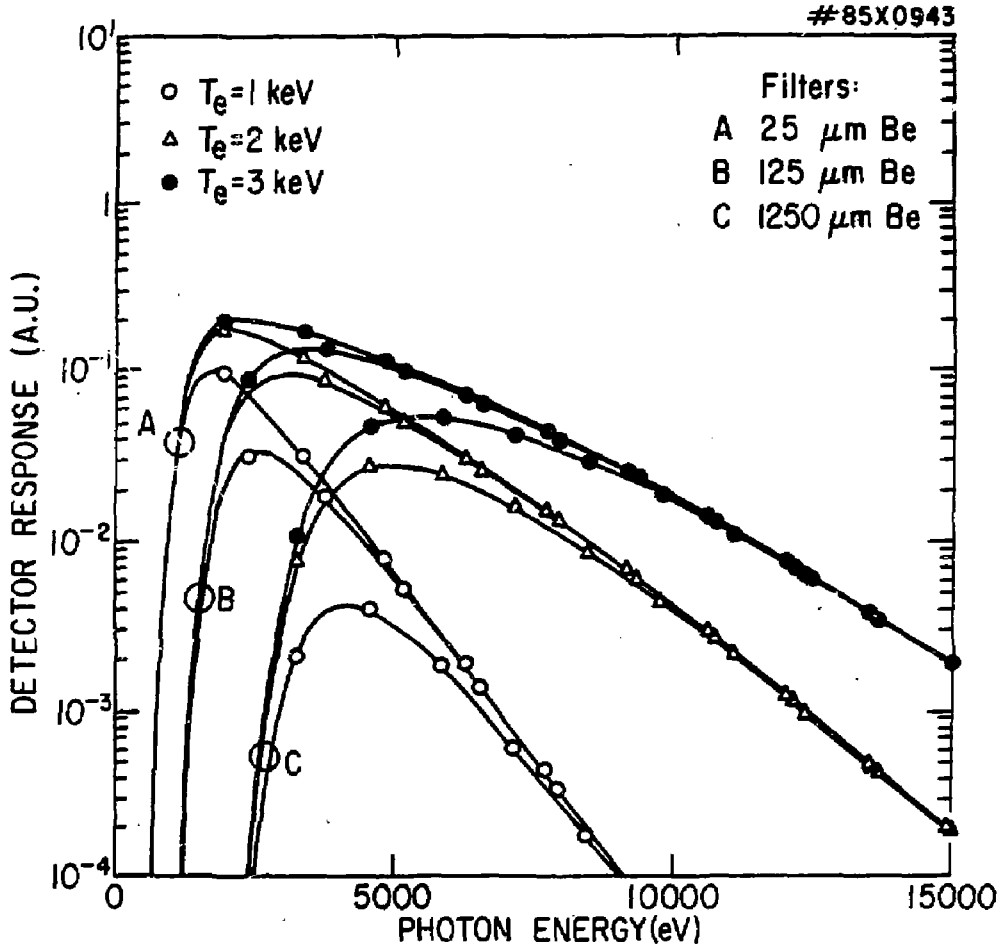
#85X0943
T_e=1 keV
T_e=2 keV
T_e=3 keV
Filters:
A 25 μm Be
B 125 μm Be
C 1250 μm Be
DETECTOR RESPONSE (A.U.)
PHOTON ENERGY(eV)
A
B
C
10^{1}
1
10^{-1}
10^{-2}
10^{-3}
10^{-4}
0
5000
10000
15000

Fig. 8

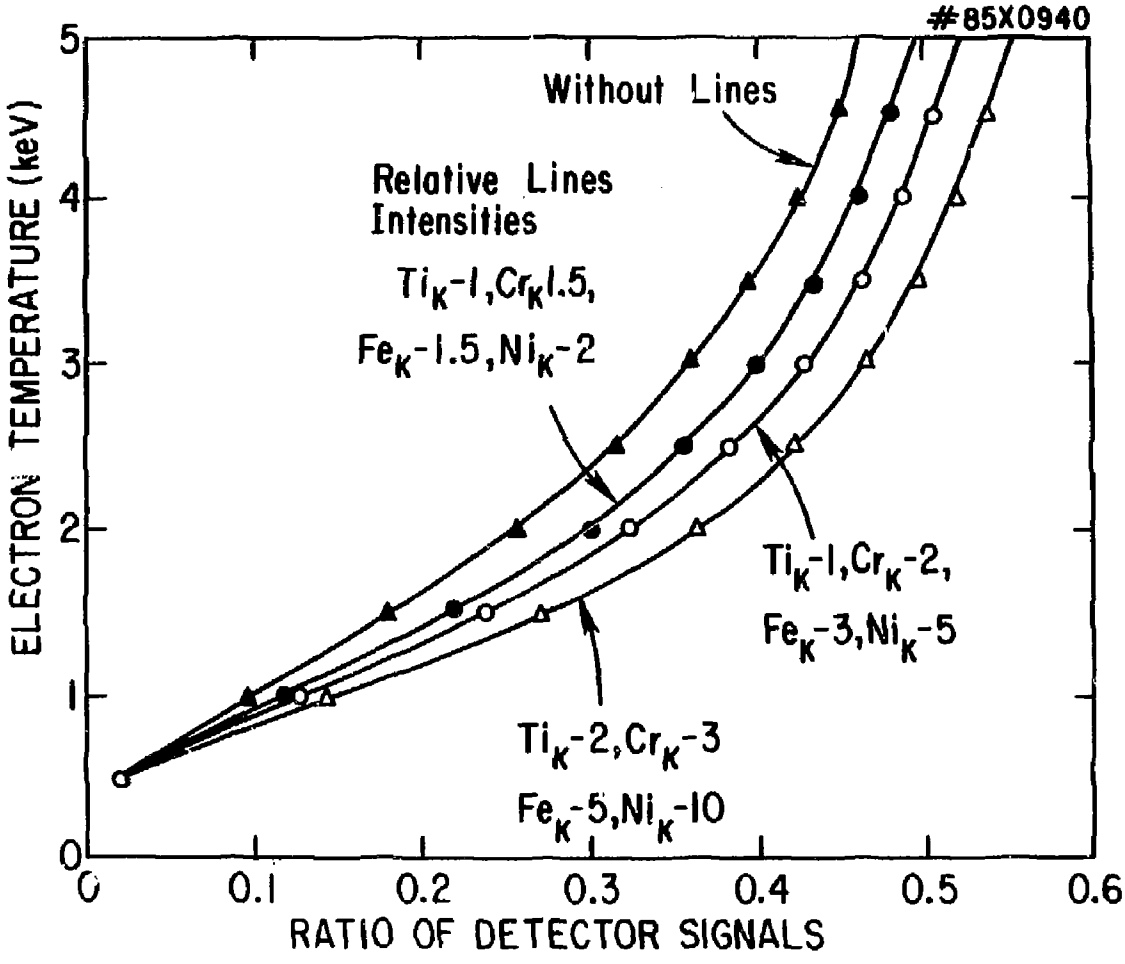
#85X0940
Without Lines
Relative Lines Intensities
Ti_K-1,Cr_K1.5,
Fe_K-1.5,Ni_K-2
Ti_K-1,Cr_K-2,
Fe_K-3,Ni_K-5
Ti_K-2,Cr_K-3
Fe_K-5,Ni_K-10
ELECTRON TEMPERATURE (keV)
RATIO OF DETECTOR SIGNALS
0
1
2
3
4
5
0.1
0.2
0.3
0.4
0.5
0.6

Fig. 9

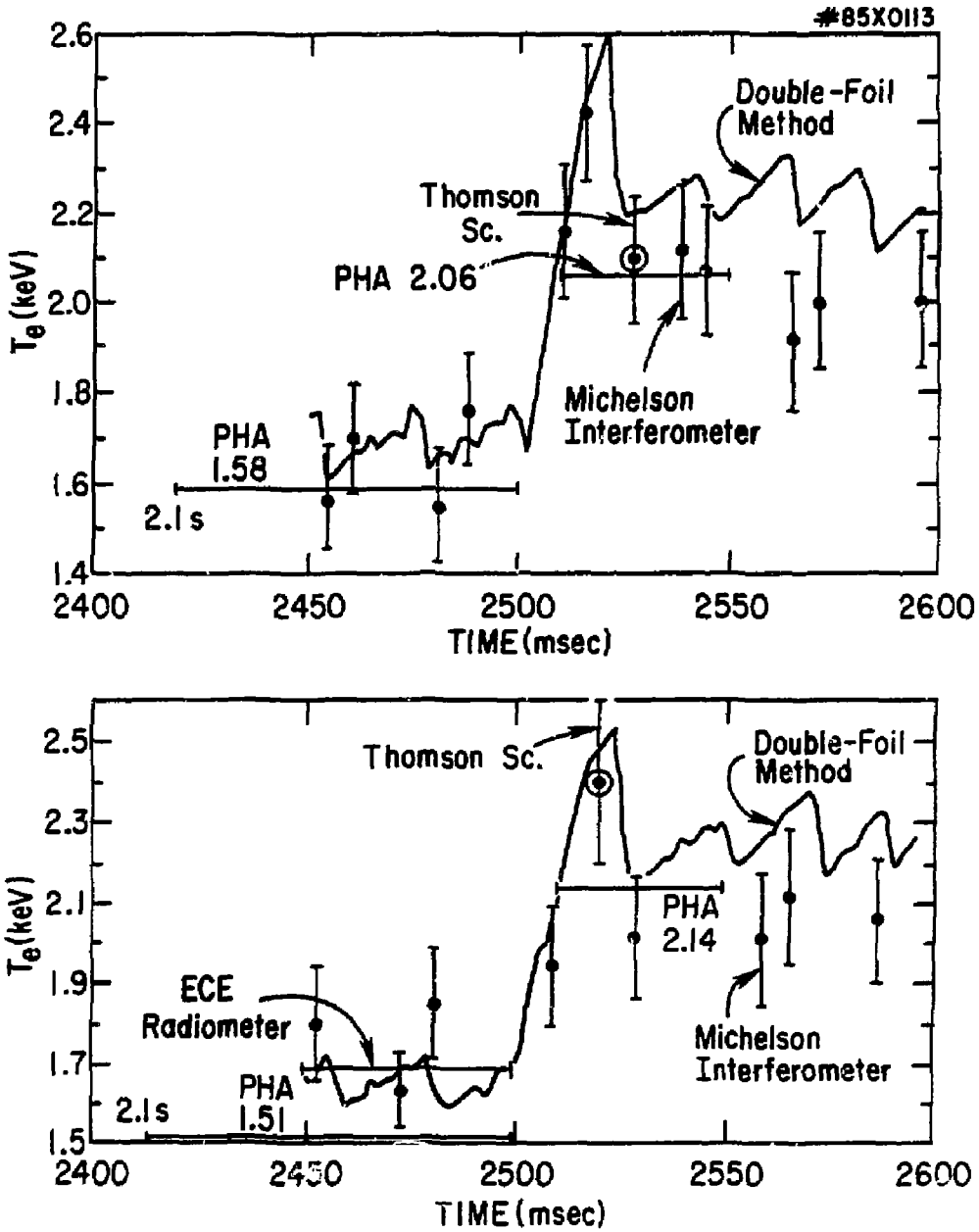
#85X0113
Double-Foil Method
Thomson Sc.
PHA 2.06
Michelson Interferometer
PHA 1.58
2.1 s
T_e(keV)
TIME(msec)
Thomson Sc.
Double-Foil Method
PHA 2.14
ECE Radiometer
Michelson Interferometer
PHA 1.51
2.1 s
T_e(keV)
TIME(msec)

Fig. 10

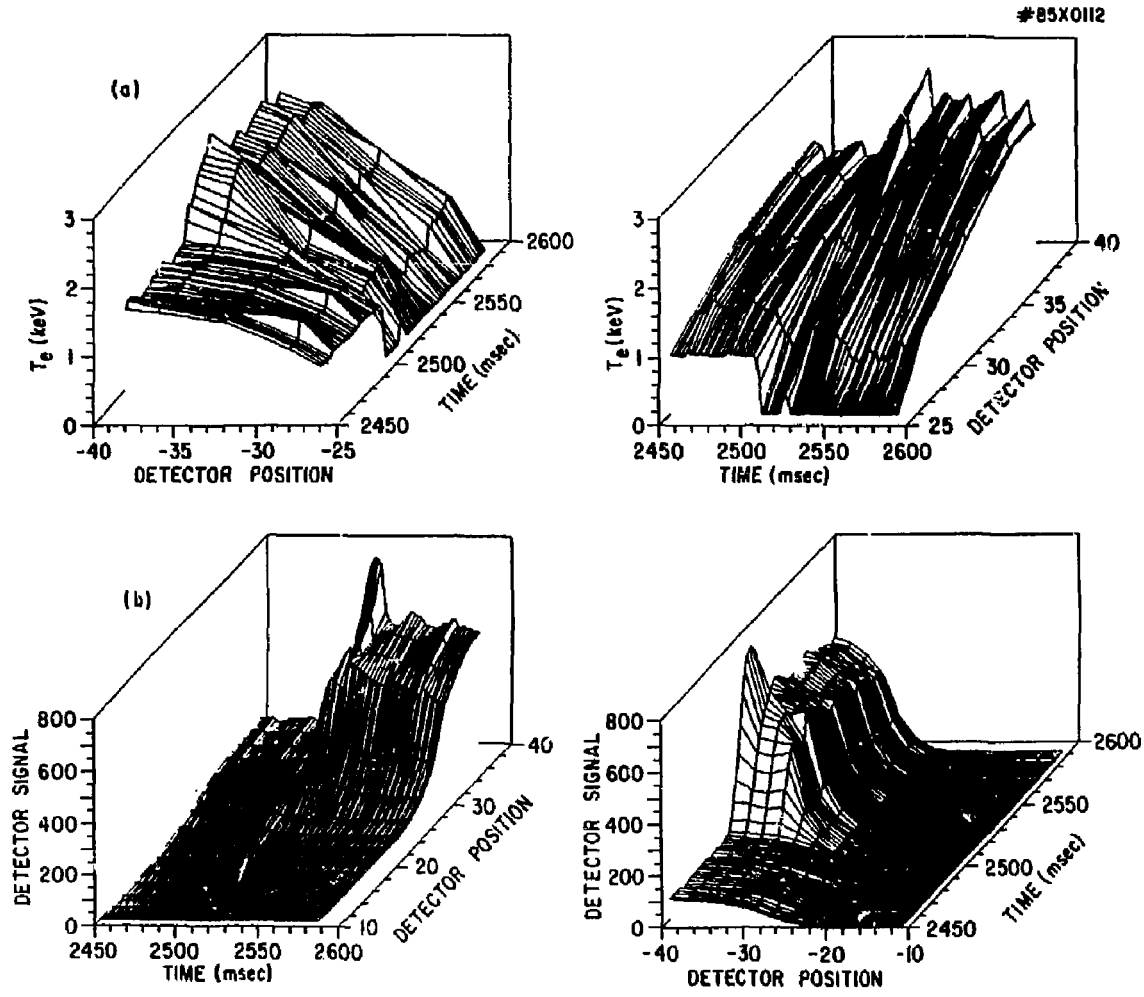
#85X0112
(a)
T_e (keV)
DETECTOR POSITION
TIME (msec)
(b)
DETECTOR SIGNAL
DETECTOR POSITION
TIME (msec)

Fig. 11a,b

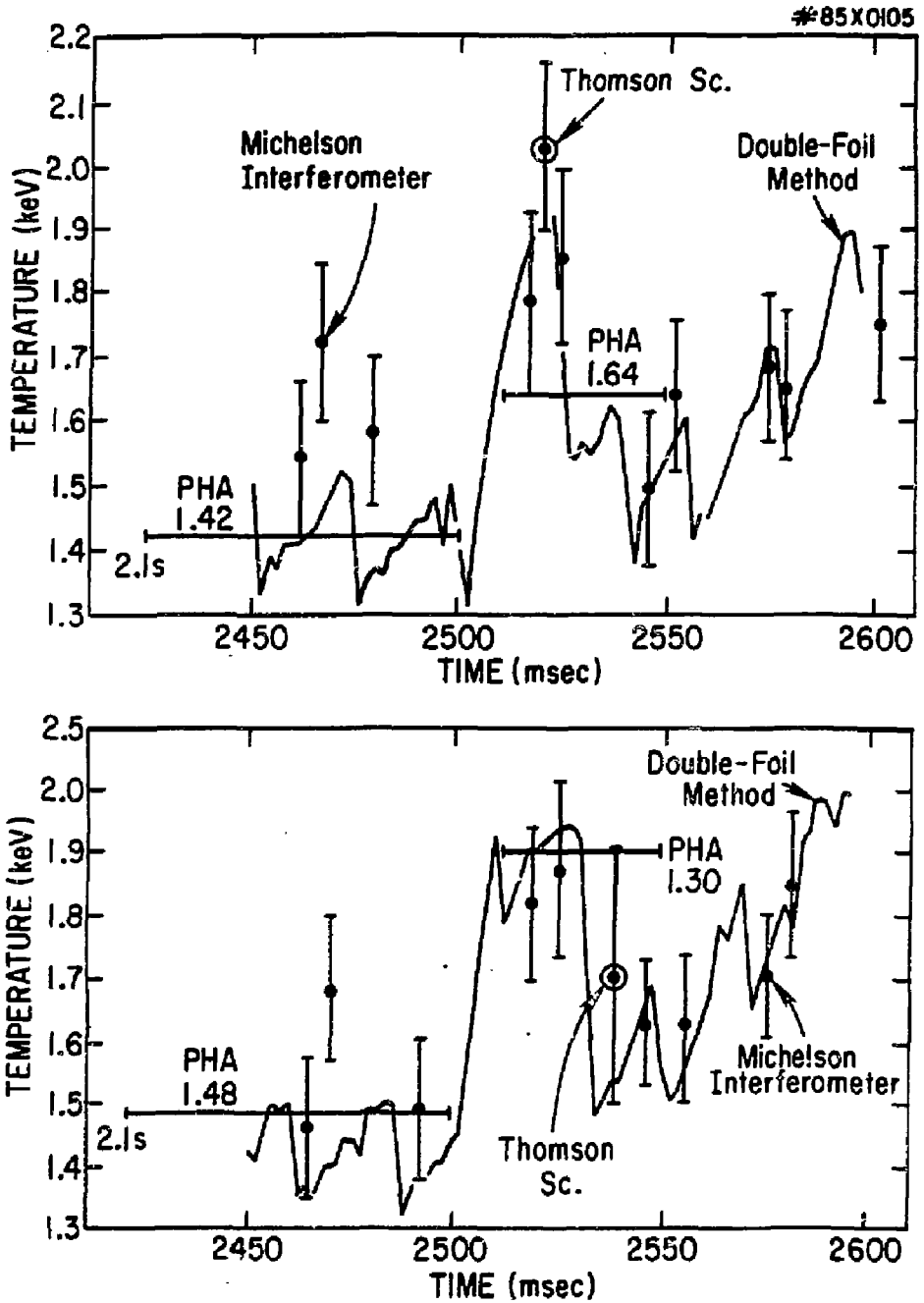
#85X0105
Thomson Sc.
Michelson Interferometer
Double-Foil Method
PHA 1.64
PHA 1.42
2.1s
TEMPERATURE (keV)
TIME (msec)
Double-Foil Method
PHA 1.30
PHA 1.48
2.1s
Michelson Interferometer
Thomson Sc.
TEMPERATURE (keV)
TIME (msec)

Fig. 12

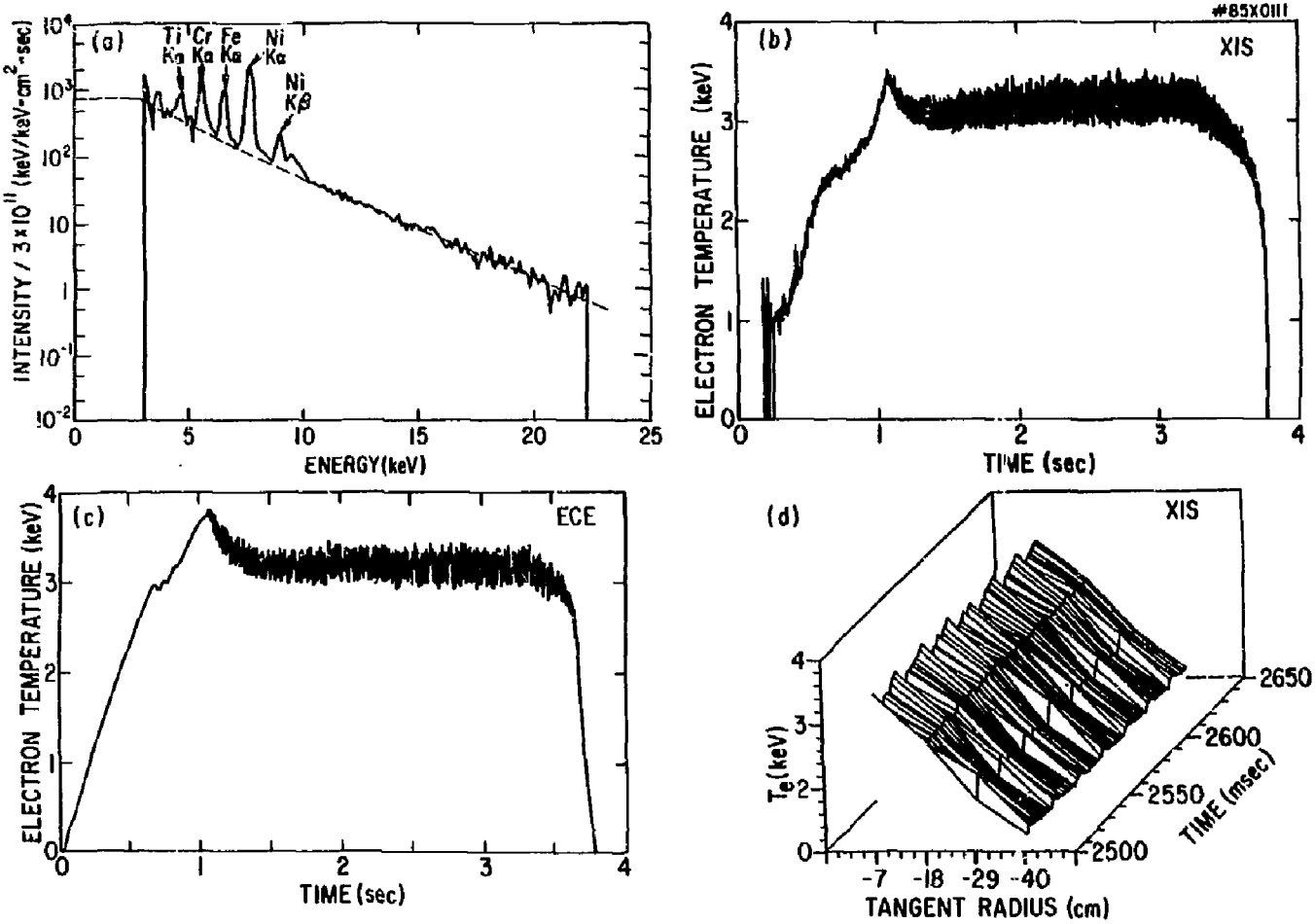
(a)
Ti Kα
Cr Kα
Fe Kα
Ni Kα
Ni Kβ
INTENSITY / 3×10^11 (keV/keV-cm^2-sec)
ENERGY(keV)
#85X0111
(b)
XIS
ELECTRON TEMPERATURE (keV)
TIME (sec)
(c)
ECE
ELECTRON TEMPERATURE (keV)
TIME (sec)
(d)
XIS
Te(keV)
TANGENT RADIUS (cm)
TIME (msec)

Fig. 13

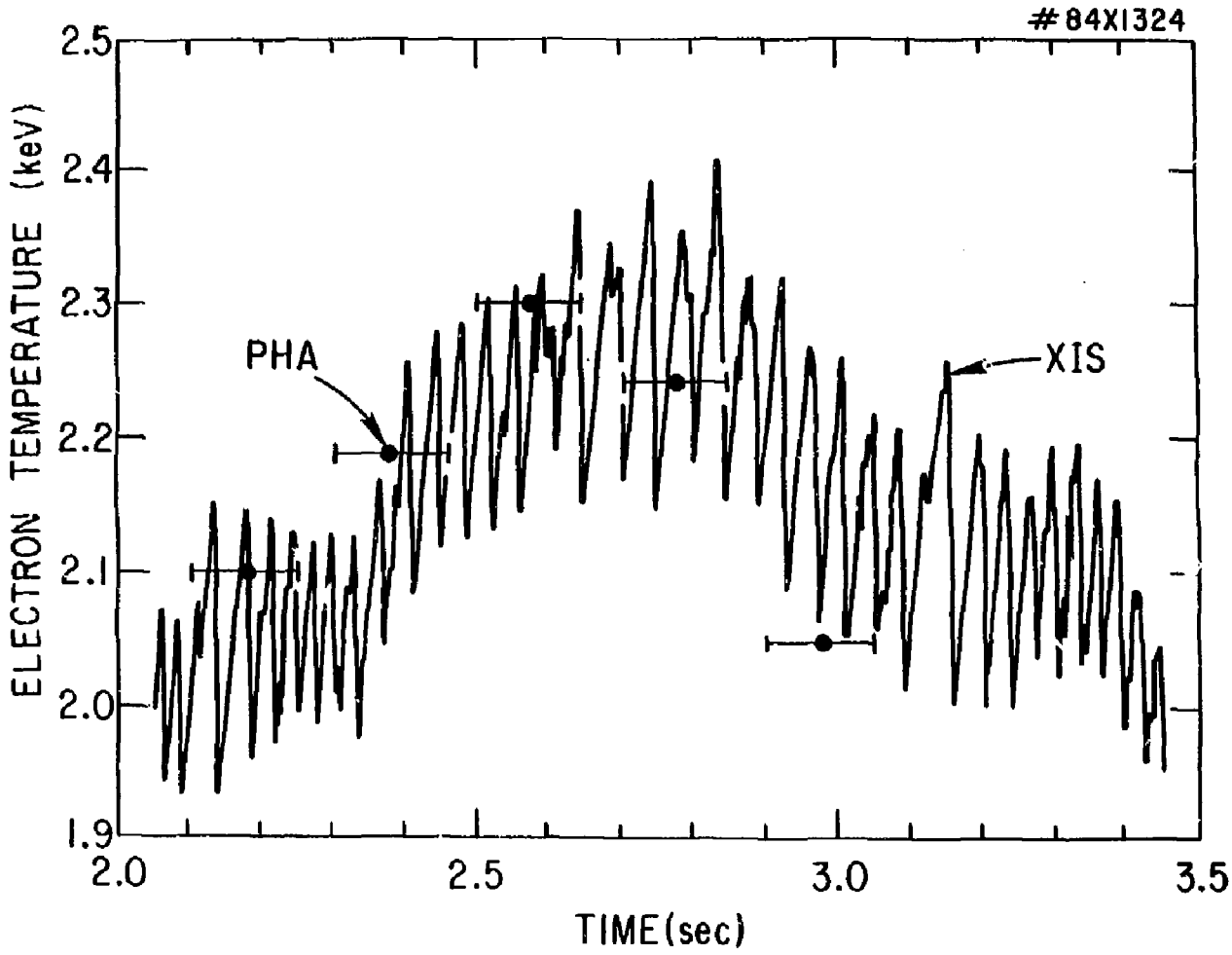
#84X1324
ELECTRON TEMPERATURE (keV)
2.5
2.4
2.3
2.2
2.1
2.0
1.9
PHA
XIS
2.0
2.5
3.0
3.5
TIME(sec)

Fig. 14

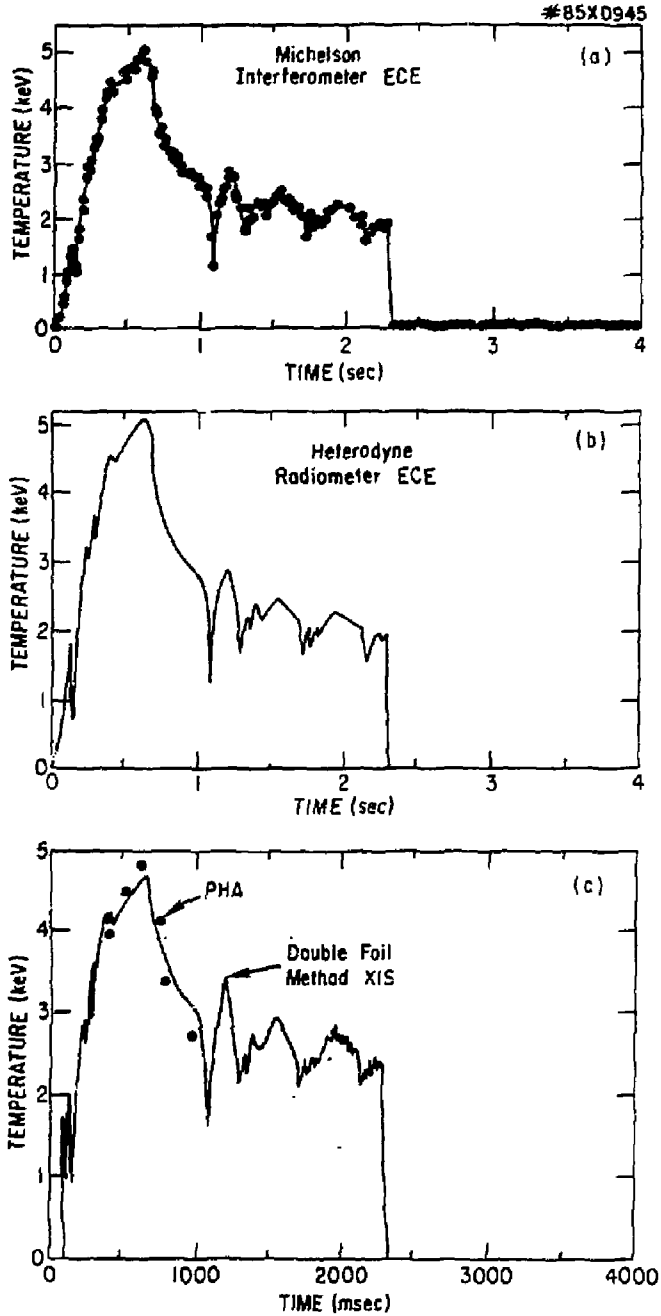
#85X0945
Michelson
Interferometer ECE
(a)
TEMPERATURE (keV)
TIME (sec)
Heterodyne
Radiometer ECE
(b)
TEMPERATURE (keV)
TIME (sec)
PHA
Double Foil
Method XIS
(c)
TEMPERATURE (keV)
TIME (msec)

Fig. 15

EXTERNAL DISTRIBUTION IN ADDITION TO UC-20

Plasma Res Lab, Austra Nat'l Univ, AUSTRALIA
Dr. Frank J. Paoloni, Univ of Wollongong, AUSTRALIA
Prof. I.R. Jones, Flinders Univ., AUSTRALIA
Prof. M.H. Brennan, Univ Sydney, AUSTRALIA
Prof. F. Cap, Inst Theo Phys, AUSTRIA
Prof. Frank Verheest, Inst theoretische, BELGIUM
Dr. D. Palumbo, Dg XII Fusion Prog, BELGIUM
Ecole Royale Militaire, Lab de Phys Plasmas, BELGIUM
Dr. P.H. Sakanaka, Univ Estadual, BRAZIL
Dr. C.R. James, Univ of Alberta, CANADA
Prof. J. Teichmann, Univ of Montreal, CANADA
Dr. H.M. Skarsgard, Univ of Saskatchewan, CANADA
Prof. S.R. Sreenivasan, University of Calgary, CANADA
Prof. Tudor W. Johnston, INRS-Energie, CANADA
Dr. Hannes Barnard, Univ British Columbia, CANADA
Dr. M.P. Bachynski, MPB Technologies, Inc., CANADA
Chalk River, Nucl Lab, CANADA
Zhengwu Li, SW Inst Physics, CHINA
Library, Tsing Hua University, CHINA
Librarian, Institute of Physics, CHINA
Inst Plasma Phys, Academia Sinica, CHINA
Dr. Peter Lukac, Komenskeho Univ, CZECHOSLOVAKIA
The Librarian, Culham Laboratory, ENGLAND
Prof. Schatzman, Observatoire de Nice, FRANCE
J. Radet, CEN-BP6, FRANCE
AM Dupas Library, AM Dupas Library, FRANCE
Dr. Tom Mual, Academy Bibliographic, HONG KONG
Preprint Library, Cent Res Inst Phys, HUNGARY
Dr. S.K. Trehan, Panjab University, INDIA
Dr. Indra Mohan Lal Das, Banaras Hindu Univ, INDIA
Dr. L.K. Chavda, South Gujarat Univ, INDIA
Dr. R.K. Chhajlani, Vikram Univ. INDIA
Dr. B. Dasgupta, Saha Inst, INDIA
Dr. P. Kaw, Physical Research Lab, INDIA
Dr. Phillip Rosenau, Israel Inst Tech, ISRAEL
Prof. S. Cuperman, Tel Aviv University, ISRAEL
Prof. G. Rostagni, Univ Di Padova, ITALY
Librarian, Int'l Ctr Theo Phys, ITALY
Miss Clelia De Palo, Assoc EURATOM-ENEA, ITALY
Biblioteca, del CNR EURATOM, ITALY
Dr. H. Yamato, Toshiba Res & Dev, JAPAN
Direc. Dept. Lg. Tokamak Dev. JAERI, JAPAN
Prof. Nobuyuki Inoue, University of Tokyo, JAPAN
Research Info Center, Nagoya University, JAPAN
Prof. Kyoji Nishikawa, Univ of Hiroshima, JAPAN
Prof. Sigeru Mori, JAERI, JAPAN
Library, Kyoto University, JAPAN
Prof. Ichiro Kawakami, Nihon Univ, JAPAN
Prof. Satoshi Itoh, Kyushu University, JAPAN
Dr. D.I. Choi, Adv. Inst Sci & Tech, KOREA
Tech Info Division, KAERI, KOREA
Bibliothek, Fom-Inst Voor Plasma, NETHERLANDS
Prof. B.S. Liley, University of Waikato, NEW ZEALAND
Prof. J.A.C. Cabral, Inst Superior Tecn, PORTUGAL
Dr. Octavian Petrus, ALI CUZA University, ROMANIA
Prof. M.A. Hellberg, University of Natal, SO AFRICA
Dr. Johan de Villiers, Plasma Physics, Nucor, SO AFRICA
Fusion Div. Library, JEN, SPAIN
Prof. Hans Wilhelmson, Chalmers Univ Tech, SWEDEN
Dr. Lennart Stenflo, University of UMEA, SWEDEN
Library, Royal Inst Tech, SWEDEN
Centre de Recherchesen, Ecole Polytech Fed, SWITZERLAND
Dr. V.T. Tolok, Kharkov Phys Tech Ins, USSR
Dr. D.D. Ryutov, Siberian Acad Sci, USSR
Dr. G.A. Eliseev, Kurchatov Institute, USSR
Dr. V.A. Glukhikh, Inst Electro-Physical, USSR
Institute Gen. Physics, USSR
Prof. T.J.M. Boyd, Univ College N Wales, WALES
Dr. K. Schindler, Ruhr Universitat, W. GERMANY
Nuclear Res Estab, Julich Ltd, W. GERMANY
Librarian, Max-Planck Institut, W. GERMANY
Bibliothek, Inst Plasmaforschung, W. GERMANY
Prof. R.K. Janev, Inst Phys, YUGOSLAVIA